Acta Crystallographica Section D
Biological Crystallography
ISSN 0907-4449

A novel cryoprotection scheme for enhancing the diffraction of crystals of recombinant cytochrome ba_3 oxidase from *Thermus thermophilus*

Laura M. Hunsicker-Wang, Ronald L. Pacoma, Ying Chen, James A. Fee and C. David Stout*

Department of Molecular Biology, The Scripps Research Institute, MB8, 10550 North Torrey Pines Road, La Jolla, CA 92037, USA

Correspondence e-mail: dave@scripps.edu

Received 5 October 2004
Accepted 21 December 2004

PDB References: cytochrome ba_3 oxidase, 1xme, r1xmesf

Cytochrome ba_3 oxidase is an integral membrane protein identified in the thermophilic bacterium *Thermus thermophilus*. The enzyme has now been expressed recombinantly and purified with a histidine tag. As such, it crystallizes under similar conditions and in the same space group ($P4_32_12$) as the native protein. A novel cryoprotection scheme is described here to obtain high-resolution diffraction from these crystals, which involves soaking in a mixture of glycerol and ethylene glycol under a layer of oil. The unit-cell parameters for these crystals are larger than the native protein, apparently deriving from increased ordering of the N-terminus and an internal loop (residues 495–500) in subunit I. Hence, compared with native cytochrome ba_3 oxidase, the recombinant His-tagged protein is accommodated in an expanded but equally well ordered lattice *via* an alternate set of specific intermolecular contacts. The structure was refined against data to 2.3 Å resolution to an R factor of 21.7% and an $R_{\rm free}$ of 23.7%.

1. Introduction

Cytochrome *c* oxidase is a terminal enzyme of respiration that catalyzes the reduction of dioxygen to water (Ferguson-Miller & Babcock, 1996; Michel *et al.*, 1998). Cytochrome ba_3 oxidase is produced by *Thermus thermophilus* when grown under low oxygen tension and is one of the most divergent members of the heme-copper oxidase super family (Calhoun *et al.*, 1994; Castresana *et al.*, 1994; Fee *et al.*, 1998; Keightley *et al.*, 1995; Zimmermann *et al.*, 1988). This protein has now been expressed, purified as a recombinant poly-histidine-tagged protein and shown to be spectrally similar to the native protein (Chen *et al.*, 2005).

Several crystal structures of cytochrome *c* oxidases have been published (Iwata *et al.*, 1995; Ostermeier *et al.*, 1997; Tsukihara *et al.*, 1995, 1996), including the native *T. thermophilus* cytochrome ba_3 (Soulimane *et al.*, 2000). Previous work provided the native cytochrome ba_3 structure at 2.4 Å resolution, in which the crystals were transformed by dehydration in order to obtain high-resolution diffraction. In this technique, a crystal drop was flooded with oil and the mother liquor was removed. A crystal was then taken from the oil drop, the diffraction monitored at room temperature until it reached an optimal resolution and then frozen. Dehydration could be achieved using ambient conditions or a dehumidifying apparatus (Kiefersauer *et al.*, 2000). Considerable variability in the unit-cell parameters was observed, with the *c* axis changing up to 20 Å (c = 160–180 Å) depending on the degree of dehydration (Soulimane *et al.*, 2000, 2003). The procedure reported here describes an alternative technically simpler cryoprotection and freezing protocol that results in excellent diffraction and a consistent *c*-axis length (∼177 Å) that is comparable to the untransformed unit-cell parameter of native cytochrome ba_3 oxidase (Soulimane *et al.*, 2003). In the crystal lattice of the recombinant His-tagged enzyme, the N-terminus of subunit I is ordered and several new crystal contacts are made that account for the ability to resolve portions of the molecule that were not modeled previously. Using our cryoprotection technique, it is now possible to study crystal structures of the recombinant protein at high resolution.

2. Materials and methods

2.1. Protein purification and crystallization

Recombinant cytochrome ba_3 was expressed and purified as described elsewhere (Chen *et al.*, 2005). Purified protein was crys-

© 2005 International Union of Crystallography
Printed in Denmark – all rights reserved

Table 1
Crystallographic analysis.

Values in parentheses are for the last shell.

Crystal	Recombinant	Native†
PDB code	1xme	1ehk
Space group	$P4_32_12$	$P4_32_12$
Unit-cell parameters (Å)		
$a = b$	114.9	112.1
c	177.1	161.4
Solvent content (%)	61.6%	59.0%
Data collection		
Total observations $>2\sigma(F)$	292061	
Unique observations $>2\sigma(F)$	46143‡	39379
Resolution (Å)	21.5–2.4 (2.46–2.4)‡	20.0–2.4 (2.49–2.4)
Mosaic spread (°)	0.3-0.6	
Redundancy	6.3 (5.0)	
Completeness (%)	98.5 (98.5)	96.3 (95.0)
$\langle I/\sigma(I)\rangle$	14.5 (2.2)	
R_{sym}	0.096 (0.663)	
Refinement‡		
Residue ranges		
Subunit I	6–562	14–495, 501–562
Subunit II	3–168	3–168
Subunit IIa	2–34	2–34
R (%)	21.7	22.2
R_{free} (%)	23.7	26.4
Observations in test set	2480	1972
R.m.s. bond lengths (Å)	0.008	0.008
R.m.s. angle deviations (°)	1.3	1.6
Average B values (Å^2)		
Protein	52.6 (756 residues, 5964 atoms)	50.6 (6143 atoms)
Cofactors	39.4 (4 residues, 112 atoms)	
Water molecules	50.9 (74 residues, 74 atoms)	45.5 (118 atoms)

† Selected values for comparison taken from PDB entry 1ehk (Soulimane *et al.*, 2000). ‡ For refinement, an additional ∼3000 reflections $>2\sigma(F)$ in the shell 2.4–2.3 Å were included (see §2.3). The data were not complete in this shell owing to anisotropy in the diffraction.

tallized by the previous protocol (Soulimane *et al.*, 2003) with some modifications. The protein was exchanged at room temperature into crystallization buffer [30 m*M* Bis-Tris pH 7.0, 100 m*M* KCl, 13 m*M* nonyl-β-D-glucopyranoside (NBG)] using ∼2 ml DEAE Sepharose equilibrated with the crystallization buffer without the KCl (equilibration buffer). The protein, diluted with equilibration buffer, was loaded onto the resin, washed with ∼5 ml equilibration buffer and eluted using ∼6 ml of the 100 m*M* KCl crystallization buffer. The protein was concentrated to ∼10 mg ml^{-1} using an Amicon concentrator; the concentration was calculated using $\varepsilon_{560-590\,nm}$ = 26 000 M^{-1} cm^{-1} for the reduced protein (Chen *et al.*, 2005) or $\varepsilon_{613-658\,nm}$ = 6300 M^{-1} cm^{-1} for the reduced − oxidized difference spectrum (Zimmermann *et al.*, 1988). The protein was centrifuged for ∼2 min at 14 000 rev min^{-1} to remove trace precipitate.

Crystals were formed by vapor diffusion from 4 µl sitting drops with 850 µl well solution (14–16% PEG 2K, 30–60 m*M* Bis-Tris pH 7.0), with 2 µl protein added to 2 µl well solution in the drop. The protein and well solutions were not mixed but allowed to slowly diffuse together, since this produced better formed crystals. Crystals formed overnight when incubated at 297 K and new crystals continued to form for around a week.

2.2. Cryoprotection and freezing

3 µl of the cryoprotection solution (15% PEG 2K, 20% glycerol, 20% ethylene glycol, 30 m*M* Bis-Tris pH 7.0, 6.5 m*M* NBG) was added to the 4 µl crystal drop. After ∼1–2 min, 25 µl of an oil mixture (9:2 mixture paraffin oil:*n*-heptane) as used in the previous work (Soulimane *et al.*, 2000) was layered over the 7 µl cryoprotected drop. The well was then resealed and left undisturbed for 1 h or longer. Crystals were removed from the aqueous phase through the oil using a nylon loop. After exposure to air for 5–10 min, the loop was plunged into liquid nitrogen. The highest resolution data came from crystals in drops incubated under oil for 2–4 h and exposed to air for 10 min. This procedure was developed by systematic variation of conditions and reagents applied to over 100 crystals, each of which was tested for diffraction characteristics.

2.3. Data collection, molecular replacement and refinement

Data were collected on beamline 11-1 at SSRL at λ = 0.98 Å, recorded with an ADSC Q315 CCD detector, processed with *MOSFLM* and scaled using *SCALA* from the *CCP*4 program package (Collaborative Computational Project, Number 4, 1994). Crystals were tetragonal bipyramidal (longest direction $\simeq$ 0.2 mm) belonging to space group $P4_32_12$, with unit-cell parameters 114.9 × 114.9 × 177.1 Å and a solvent content of 61.7% (Table 1).

Molecular replacement was performed using *MOLREP* (Collaborative Computational Project, Number 4, 1994) starting with the native crystal structure (PDB code 1ehk) as a model; the best solution had R = 35.5% and a correlation coefficient of 0.739. The *MOLREP* model was refined using *CNS* (Brünger *et al.*, 1998) in concert with *Xfit* (McRee, 1999) to interpret unbiased $2|F_o| - |F_c|$, $|F_o| - |F_c|$ and composite omit electron-density maps. An additional eight amino acids could be built into density extending from the N-terminus of subunit I. A loop missing from the native model in subunit I, residues 495–500, was also clearly defined in the density. Some repositioning at the N- and C-termini of subunits II and IIa was also necessary.

Diffraction data extended to 2.1 Å, but were not complete to that resolution. Data were therefore scaled to 2.4 Å, even though there was significant information at higher resolution. Upon calculating several maps and building most of the model, the data were rescaled to 2.3 Å and an additional 3000 reflections in the 2.4–2.3 Å shell with $|F| > 2\sigma(F)$ were included in the refinement (Table 1). Appropriate stereochemical restraints were employed for the heme *b*, heme a_3, Cu_B and Cu_A moieties. Patches were added in *CNS* topology and parameter files (Brünger *et al.*, 1998) to accommodate metal-ion ligands. In particular, the His384 N^{ε}—Fe target bond length was set to 2.50 Å based on the fit of this residue and adjoining α-helix residues to unbiased σ_A-weighted $2|F_o| - |F_c|$ omit maps calculated following full *CNS* refinement in the absence of restraints on this bond. The restraint was also systematically altered in several steps of ±0.1 Å. The model refined with the 2.50 Å restraint resulted in the least difference density between the Fe and His384 N^{ε} atoms in σ_A-weighted $|F_o| - |F_c|$ omit maps

3. Results and discussion

3.1. Cryoprotection

In addition to the published activity and spectral studies (Chen *et al.*, 2005), the ability of the recombinant protein to crystallize and diffract to a resolution comparable to the native protein demonstrates that the recombinant protein is correctly assembled. In a number of trials, crystals of the recombinant protein treated as the previously reported native crystals (Soulimane *et al.*, 2000, 2003) did not diffract beyond ∼4 Å. The requisite extent and variability of the *c*-axis shrinkage at room temperature before freezing made it difficult to reproduce. Thus, we developed a new cryoprotection scheme, outlined above, which produces 2.3 Å diffraction. The procedure calls for bathing the crystals in a solution with suitable additives and does not require manipulation of the crystals until they are ready to be frozen. However, like the procedure for native crystals, the crystals are allowed to dehydrate at room temperature under the paraffin oil:*n*-heptane mixture before freezing.

Table 2
Hydrogen-bonding summary.

See supplementary material for details. Contacts were defined as a hydrogen bond when the distance is ≤3.6 Å between donor and acceptor protein atoms with a D—H—A angle in the range 140–180°.

	No. hydrogen bonds†	
Type of hydrogen bond	Recombinant	Native
Main chain–main chain	3	2
Main chain–side chain	4	4
Side chain–side chain	2	2
Total	9	8

† Contacts with respect to the reference molecule. Crystal-packing contacts were determined using the web-based program *CryCo* (Sobolev *et al.*, 1999).

3.2. Comparison and crystal packing

Overall, the structure of the recombinant protein is similar to the native protein, with an r.m.s.d. of 0.21 Å (overall C^{α}); the only large differences are at the subunit I N-terminus and the residue 495–500 loop. The subunit I N-terminal α-helix could be extended by eight amino acids, but the histidine tag and amino acids 1–7 are still disordered. The loop of residues 495–500 interacts with the extended N-terminus, apparently stabilizing the loop.

Comparison of the crystal packing between the native and recombinant molecules shows less compression of the *c* axis (162 Å compared with 177 Å; Table 1). This affects molecules that align both parallel and normal to the [110] direction. The extended subunit I N-terminus precludes the more compressed *c* axis owing to lattice contacts (Fig. 1). This may also allow the detergent micelle surrounding the membrane-spanning region for the recombinant protein to be larger, although the same detergent is present in both crystal forms. Thus, it appears that the presence of the His tag on the N-terminus of the recombinant protein prevents closer packing along the *z* direction. In spite of this, under the given cryoprotection condition, the alternative packing arrangement becomes well ordered. Hence, there are two distinctly different sets of packing contacts that result in a well ordered lattice for this large integral membrane protein (Fig. 1).

An analysis of the crystal contacts shows that the recombinant protein has one more hydrogen bond than the native and that it is a

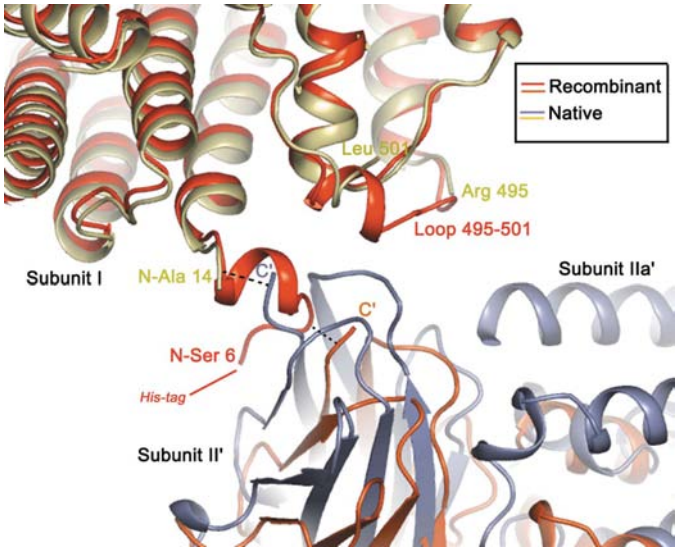

Figure 1
Comparison of crystal-packing interactions at the subunit I N-termini of the native and recombinant proteins. Ribbon diagrams of overlaid recombinant (red) and native (gold) compared with symmetry-related recombinant (orange) and native (slate blue) proteins. Dotted lines indicate representative crystal contacts between the symmetry pairs. The eight molecules of each unit cell were generated by the $P4_32_12$ symmetry within their respective cells and the packing arrangements were superimposed with respect to a reference copy (red and gold) using the *LSQKAB* utility from the *CCP*4 program suite (Collaborative Computational Project, Number 4, 1994). The recombinant protein with its more ordered N-terminus would be in steric conflict in the compressed unit cell of the native protein; nevertheless, the His tag remains disordered in the space between molecules. The more ordered N-terminus also interacts with the ordered loop of residues 495–501.

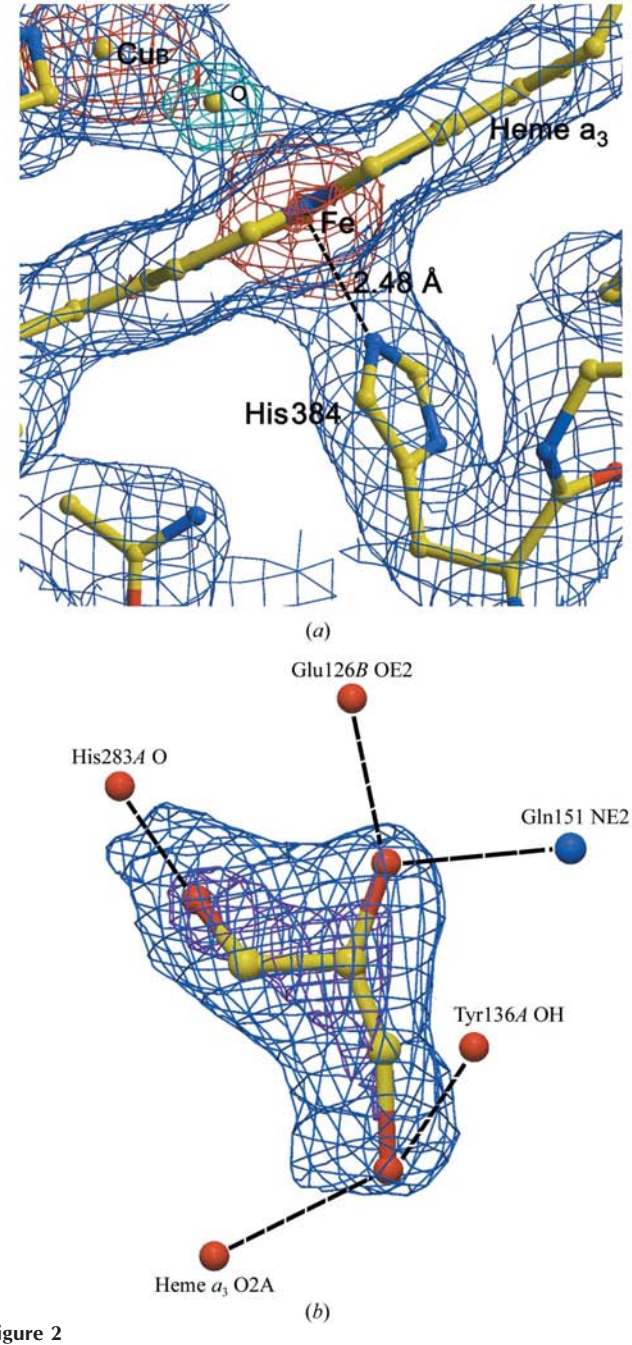

Figure 2
Electron density at the heme a_3 site and for bound glycerol. (*a*) Heme a_3 site depicting the 2.48 Å distance between His384 N^{ε} and Fe (black dashed line). Contour levels are 1σ (blue) and 5σ (red) for $2|F_o| - |F_c|$ electron density and 5σ (cyan) for $|F_o| - |F_c|$ positive difference density for the bridging O atom. Distances between the bridging O atom and Fe and Cu_B are 2.44 and 2.07 Å, respectively. (*b*) Unbiased $2|F_o| - |F_c|$ electron-density map of the bound glycerol molecule hydrogen bonded to the O2A atom of the propionate group of heme a_3, Tyr136*A* OH, His283*A* O, Glu126*B* OE2 and Gln151*B* NE2. Contour levels are 1σ (blue) and 2.5σ (purple).

main chain to main chain (N to O) interaction (Table 2 and supplementary material[1]). This type of hydrogen bond has been shown to be important in stabilizing protein crystal lattices (Derewenda, 2004). Although there are a comparable number of interactions, only one crystal contact is retained in both structures (Ala172*A* O to Arg560*A* N, ∼3.0 Å). Eight 'new' contacts are made in the recombinant structure; six at the N-terminus of subunit I, one involving the ordered 495–500 loop and one side-chain interaction arising from a different rotamer. Two of the crystal contacts occurring only in the native crystal are 'replaced' by intramolecular hydrogen bonds. Consequently, all of the hydrogen-bonding contacts of the compressed native cell are compensated through formation of new contacts in the larger recombinant cell and a new main-chain contact is formed. The effect of this arrangement is a crystal lattice exhibiting comparable resolution, *B* values and number of ordered H_2O molecules for the recombinant His-tagged protein (Table 1).

3.3. Novel features of the recombinant structure

The O atom found bridging Fe of heme a_3 and Cu_B is resolved as an 8σ peak in the difference Fourier map (Fig. 2*a*), with comparable bond lengths and angles to the native structure (Soulimane *et al.*, 2000). The water structure is also well defined within the integral membrane domain and near the heme a_3 and Cu_A centers. The 74 water molecules refined all occur as $>5\sigma$ peaks in difference maps (Table 1).

One notable difference between the native and recombinant structures is the heme a_3—Fe···His384 N^{ε} bond distance. In the native crystal, an unusually long distance of 3.31 Å was reported; in the recombinant crystal structure this distance is 2.48 Å (Fig. 2*a*). An overlay of the two models shows that the difference in this area is localized to Gly383-His384-Phe385. The distances between the native and recombinant C^{α} atoms for residues Gly383, His384 and Phe385 are 0.43, 0.56 and 0.33 Å, respectively (compared with the overall r.m.s.d. of 0.21 Å).

A further novelty of this structure is the presence of an ordered glycerol molecule near the heme a_3-Cu_B site (Fig. 2*b*). The glycerol OH groups are hydrogen bonded to several groups adjacent to the heme a_3-Cu_B site. The binding of glycerol may explain the stability of the crystals in the cryoprotection mixture and provide a reason for the necessary long incubation time before freezing. Secondly, in terms of the enzyme's mechanism, it implies that the water-exit pathway is large and flexible enough to accommodate the glycerol molecule in the region near the active site.

We would like to acknowledge the assistance of Justin Chartron in developing and testing the different cryoprotection additives. We would also like to thank the staff of SSRL for excellent beamline support. This work was supported by NIH grants GM 35342 (JAF) and GM61545 (CDS).

[1] Supplementary material has been deposited in the IUCr electronic archive (Reference: TS5039). Details for accessing these data are described at the back of the journal.

References

Brünger, A. T., Adams, P. D., Clore, G. M., DeLano, W. L., Gros, P., Grosse-Kunstleve, R. W., Jiang, J.-S., Kuszeweski, J., Nilges, M., Pannu, N. S., Read, R. J., Rice, L. M., Simonson, T. & Warren, G. L. (1998). *Acta Cryst.* D**54**, 905–921.

Calhoun, M. W., Thomas, J. W. & Gennis, R. B. (1994). *Trends Biochem. Sci.* **19**, 325–330.

Castresana, J., Lubben, M., Saraste, M. & Higgins, D. G. (1994). *EMBO J.* **13**, 2516–2525.

Chen, Y., Hunsicker-Wang, L. M., Pacoma, R. L., Luna, E. & Fee, J. A. (2005). In the press.

Collaborative Computational Program, Number 4 (1994). *Acta Cryst.* D**50**, 760–763.

Derewenda, Z. S. (2004). *Structure*, **12**, 529–535.

Fee, J. A., Todaro, T. R. & Sanders, D. (1998). *Cah. Biol. Mar.* **39**, 351–354.

Ferguson-Miller, S. & Babcock, G. T. (1996). *Chem. Rev.* **96**, 2889–2907.

Iwata, S., Ostermeier, C., Ludwig, B. & Michel, H. (1995). *Nature (London)*, **376**, 660–669.

Keightley, J. A., Zimmermann, B. H., Mather, M. W., Springer, P., Pastuszyn, A., Lawrence, D. M. & Fee, J. A. (1995). *J. Biol. Chem.* **270**, 20345–20358.

Kiefersauer, R., Than, M. E., Dobbek, H., Gremer, L., Melero, M., Strobl, S., Dias, J. M., Soulimane, T. & Huber, R. (2000). *J. Appl. Cryst.* **33**, 1223–1230.

McRee, D. E. (1999). *J. Struct. Biol.* **125**, 156–165.

Michel, H., Behr, J., Harrenga, A. & Kannt, A. (1998). *Annu. Rev. Biophys. Biomol. Struct.* **27**, 329–356.

Ostermeier, C., Harrenga, A., Ermler, U. & Michel, H. (1997). *Proc. Natl Acad. Sci. USA*, **94**, 10547–10553.

Sobolev, V., Sorokine, A., Prilusky, J., Abola, E. E. & Edelman, M. (1999). *Bioinformatics*, **15**, 327–332.

Soulimane, T., Buse, G., Bourenkov, G. B., Bartunik, H. D., Huber, R. & Than, M. E. (2000). *EMBO J.* **19**, 1766–1776.

Soulimane, T., Kiefersauer, R. & Than, M. E. (2003). *Membrane Protein Purification and Characterization: A Practical Guide*, edited by C. Hunte, G. von Jagow & H. Schägger, pp. 229–251. Amsterdam: Academic Press.

Tsukihara, T., Aoyama, H., Yamashita, E., Tomizaki, T., Yamaguchi, H., Shinzawa-Itoh, K., Nakashima, R., Yaono, R. & Yoshikawa, S. (1995). *Science*, **269**, 1069–1074.

Tsukihara, T., Aoyama, H., Yamashita, E., Tomizaki, T., Yamaguchi, H., Shinzawa-Itoh, K., Nakashima, R., Yaono, R. & Yoshikawa, S. (1996). *Science*, **272**, 1136–1144.

Zimmermann, B. H., Nitsche, C. I., Fee, J. A., Rusnak, F. & Munck, E. (1988). *Proc. Natl Acad. Sci. USA*, **85**, 5779–5783.